AIAA JOURNAL
Vol. 33, No. 2, February 1995

Postbuckling Compressive Strength of Graphite/Epoxy Laminated Cylindrical Panels Loaded in Compression

J. H. Kweon,* C. S. Hong,† and I. C. Lee‡
Korea Advanced Institute of Science and Technology, Taejon 305-701, Republic of Korea

The postbuckling compressive strength and collapse phenomena of composite laminated cylindrical panels with various fiber angles and width-to-length ratios are characterized by the nonlinear finite element method. For the iteration and load increment along the postbuckling equilibrium path, a modified arc-length method in which the effect of stress unloading due to failure can be considered is introduced. In the progressive failure analysis, the maximum stress criterion and complete unloading model are used. Validity of present finite element results are verified by experiment for $[0_3/90]_S$ cylindrical panel and $[0/90/\pm 45]_S$ plate. The postbuckling compressive strength of composite laminated cylindrical panels is independent of the initial buckling stress but high in the panel with large value of the bending stiffness in axial direction. In several of the cylindrical panels, it is observed that the prebuckling compressive failures occur and directly result in collapse before buckling.

Nomenclature

A	= cross-sectional area of cylindrical panel
D_{11}	= bending stiffness in axial direction
$[D]$	= stiffness matrix in global coordinate system
$\{F_0\}$	= force-distribution vector
$[K_T]$	= tangent stiffness matrix
k	= arc-length increment ratio
P_{cr}, P_{col}, P_{com}	= buckling stress, postbuckling compressive strength, and prebuckling compressive strength
R, L, d, t	= radius, length, width, and thickness of cylindrical panel
T_i	= surface traction
Δ, Δ_t	= increment, total summation of increment in a load step
$\Delta\ell$	= arc length
δ	= variational operator
ε_{ij}	= Green strain
λ	= load parameter

Superscript

n	= iteration number

Introduction

ADVANCED composite materials such as graphite/epoxy have been widely used in aircraft and spacecraft structures due to their design versatility as well as high specific stiffness and strength. Since cylindrical panel is commonly used structural element, a great number of studies have been conducted to characterize the mechanical behavior of composite laminated cylindrical panels. Characterization of the buckling and postbuckling behavior has been the most important topic.[1,2]

To design the composite cylindrical panel safely and efficiently, two critical questions should be answered: the first question is when buckling occurs, and the second question is when the structure collapses. The first concern is with the buckling load and the other is with the collapse load, namely, postbuckling compressive strength. However, most of the previous buckling studies have been focused on the prediction of the initial buckling load and initial buckling mode shape.[3–8] Although a limited number of papers on postbuckling behavior are available, they are either experimental studies or do not consider the effect of failure on the postbuckling behavior.[9,10] Only one paper, on the postbuckling progressive failure response of the laminated flat plates was reported, by Engelstad et al.,[11] and the finite element method (FEM) or other numerical results for postbuckling compressive strength of composite laminated cylindrical panel under compression have not been found to this day. As a result, in the authors' previous paper,[12] as a preliminary work to answer the second question on the postbuckling compressive strength, an improved load-increment method based on the arc-length scheme was presented, and the postbuckling behavior of composite laminated cylindrical panels under compression was investigated without consideration of failure effect.

In this paper, a progressive failure model is introduced into the nonlinear finite element method and the postbuckling compressive strength of graphite/epoxy laminated cylindrical panels under compression is characterized. In the progressive failure analysis, the maximum stress criterion and the complete unloading model are used. Because it was found that the conventional arc-length methods can not be directly applied to the progressive failure analysis using the complete unloading model, a new method to control the arc length is presented for the postbuckling failure analysis. For the finite element modeling of a laminated cylindrical panel, the shear deformable eight-node degenerated shell element is adopted, and the updated Lagrangian description method is used. The finite element results are compared with experimental results for $[0_3/90]_S$ cylindrical panel and $[0/\pm 45/90]_S$ plate. As numerical examples, postbuckling compressive strength and collapse characteristics of $[0/90/\pm\theta]_S$ laminated cylindrical panels with various fiber angles and width-to-length ratios are predicted.

Finite Element Analysis

Nonlinear Finite Element Formulation

In the case of no body force, principle of virtual work at an arbitrary $(n+1)$st equilibrium state can be written in terms of increments of the second Piola-Kirchhoff stress S_{ij} and the Green strain ε_{ij} taking the configuration at nth equilibrium state[3]

$$\int\int\int_{V^n} \left(\sigma_{ij}^n + \Delta S_{ij}\right)\delta(\Delta\varepsilon_{ij})\,dV - \int\int_{S_T^n} \left(T_i^n + \Delta T_i\right)\delta(\Delta u_i)\,dS = 0 \tag{1}$$

where σ_{ij}, e_{ij}, T_i, u_i, and δ are the Cauchy stress, infinitesimal strain, surface traction, displacement, and variational operator, respectively.

Received Feb. 8, 1994; presented as Paper 94-1341 at the AIAA/ASME/ASCE/AHS/ASC 35th Structures, Structural Dynamics, and Materials Conference, Hilton Head, SC, April 18–20, 1994; revision received Sept. 28, 1994; accepted for publication Oct. 2, 1994.

*Currently Senior Engineer, Samsung Aerospace Industries, Ltd.
†Professor, Department of Aerospace Engineering. Member AIAA.
‡Research Assistant, Department of Aerospace Engineering.

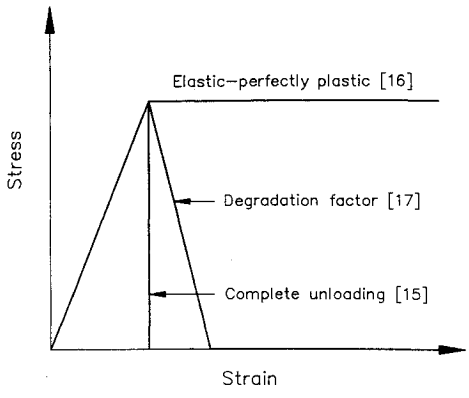

Fig. 1 Schematic diagram for various stiffness degradation models.

From Eq. (1), the finite element equation for the composite laminated cylindrical panel is derived as

$$[K_T]\{\Delta u^{n+1}\} = -\{\Delta P(\lambda^{n+1})\} \tag{2}$$

where

$$[K_T] = \int\int\int_{V^n} \left[B_L^n\right]^T [D^n] \left[B_L^n\right] dV + \int\int\int_{V^n} \left[B_{NL}^n\right]^T [\bar{\sigma}^n] \left[B_{NL}^n\right] dV \tag{3}$$

$$\{\Delta P(\lambda^{n+1})\} = \{R^{n+1}\} - \lambda^{n+1}\{F_0\} \tag{4}$$

$$\{R^{n+1}\} = \int\int\int_{V^n} \left[B_L^n\right]^T \{\sigma^n\} dV \tag{5}$$

In Eqs. (4) and (5), $[B_L]$, $[B_{NL}]$, $\{\sigma\}$, and $[\bar{\sigma}]$ can be found in Ref. 13. Also, λ and $\{F_0\}$ are load parameter and external force-distribution vector, respectively. $[D]$ is the stress-strain relation matrix in the global rectangular coordinate system.[3]

The finite element used is the eight-node degenerated shell element, and the first-order shear deformation theory is applied to the element. Incremental displacement fields in the element are expressed as

$$\begin{Bmatrix} \Delta u \\ \Delta v \\ \Delta w \end{Bmatrix} = \sum_{n=1}^{8} H_n(\xi, \eta) \begin{Bmatrix} \Delta u_n \\ \Delta v_n \\ \Delta w_n \end{Bmatrix} + \frac{1}{2} \sum_{n=1}^{8} H_n(\xi, \eta) t_n \zeta \{\Delta V_{n\zeta}\} \tag{6}$$

where ξ, η, and ζ are local coordinates in the element. $H_n(\xi, \eta)$, t_n, and $\{\Delta V_{n\zeta}\}$ are shape function, thickness, and increment of the vector in the ζ direction at the nth node, respectively.

Failure Analysis

In this finite element analysis, calculated stress is based on the global Cartesian coordinate system. Therefore, the stress components are to be transformed into the principal material direction through the elemental coordinate system. Then, to estimate the failure in the principal material direction of each layer of each element, the maximum stress criterion[14] is applied to the average stresses; therefore the failure modes can be known in the criterion. Also, to conservatively estimate the postbuckling load-carrying capacity, it is assumed that the stress corresponding to failure mode of each layer is completely unloaded and the stiffness becomes zero. Concept of the complete unloading failure model is shown in Fig. 1.

The failure is estimated once for one load step after the load step converges, then the stress corresponding to the failure mode is unloaded instantaneously. Therefore, if failure occurs at a previous load step, the unbalanced force due to the stress unloading is induced, and the force equilibrium at the first iteration of present load step is broken. For the postbuckling failure analysis, the effect of the deformation due to the failure-induced unbalanced force should be considered in the arc-length method.

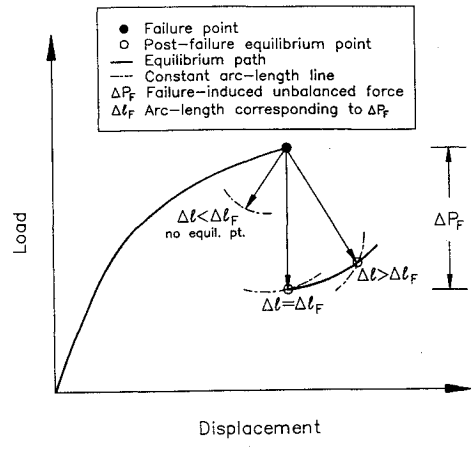

Fig. 2 Schematic diagram for modified arc-length method.

Modified Arc-Length Method

In the conventional arc-length methods, the magnitude of total deformation in a given load step $\{\Delta_t u\}$ is determined by the arc length $\Delta\ell$ as[14]

$$\{\Delta_t u\}^T \{\Delta_t u\} = (\Delta\ell)^2 \tag{7}$$

and the incremental load-parameter $\Delta\lambda^{n+1}$ at the $(n+1)$st iteration is given by

$$(\Delta\lambda^{n+1}) = (-B \pm \sqrt{B^2 - 4AC})/(2A) \tag{8}$$

where A, B, and C are given in Ref. 18.

As mentioned earlier, in the analysis with consideration of the stress unloading in the failed layer, the unbalanced force due to the failure is induced as shown in Fig. 2. Then, in addition to the deformation by the increment of external force, the deformation due to the failure-induced unbalanced force occurs. Therefore, for the incremental load-parameter to have the real solution, the arc-length in Eq. (7) must be large enough to allow the deformation corresponding to the failure-induced unbalanced force to occur. If not so, Eq. (8) can not have the real solution. Nevertheless, in the conventional arc-length methods, if Eq. (8) does not have the real solution, it is recommended only to reduce the arc-length to $\Delta\ell'$ as

$$\Delta\ell' = k\Delta\ell, \qquad 0 < k < 1 \tag{9}$$

In this paper, if Eq. (8) has a negative discriminant, the magnitude of the failure-induced unbalanced force $\{\Delta P_F\}$ and the arc-length corresponding to the force $\Delta\ell_F$ are calculated first,

$$\Delta\ell_F = \left[\{\Delta u_F\}^T \{\Delta u_F\}\right]^{\frac{1}{2}} \quad \text{with} \quad \{\Delta u_F\} = [K_T]^{-1}\{\Delta P_F\} \tag{10}$$

Then, if the present arc-length is smaller than $\Delta\ell_F$ [in which case Eq. (8) has a negative discriminant], the arc length is increased to $\Delta\ell'$ as

$$\Delta\ell' = k\Delta\ell, \qquad k > (\Delta\ell_F)/(\Delta\ell) \tag{11}$$

Ideally, the value of k is recommended to be equal to $\Delta\ell_F/\Delta\ell$. However, $k = 1.1(\Delta\ell_F)/(\Delta\ell)$ is recommended for the numerical stability. In the present postbuckling failure analysis of laminated cylindrical panels, most of the restarts after the first ply failure were due to the failure-induced unbalanced force.

Experiment

As shown in Fig. 3, boundary conditions are clamped on the curved edges and simply supported along the straight edges. To meet these boundary conditions, two pairs of fixtures are fabricated. Specimens are cured in an autoclave according to the manufacturer's recommended procedures. The specimens are machined to 150 × 157 mm in the longitudinal and circumferential dimensions, respectively, and the ends of the specimens are machined flat and parallel to permit uniform compressive loading. The experimental setup

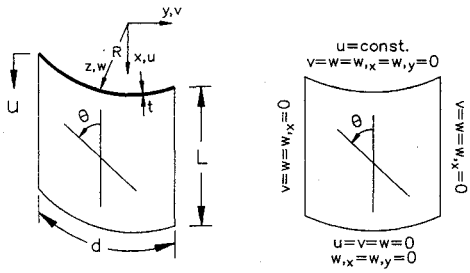

R/t=150, R=L=150mm
d/L=1.047, 0.524, 0.262

Fig. 3 Panel geometry and boundary conditions.

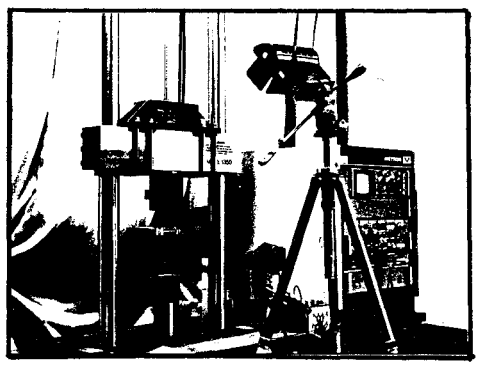

Fig. 4 Experimental setup.

is shown in Fig. 4 and INSTRON (model 1350) is used for the test. One side of each specimen is painted white to reflect light so that the shadow moire technique could be used to monitor the out-of-plane displacement patterns of the specimens during the experiments.

Results and Discussion

Problem Description

Composite cylindrical panels considered as numerical examples have the stacking sequence of $[0/90/\pm\theta]_S$, with various fiber angles on θ and width-to-length ratios. The fiber angle θ is defined as the counter-clockwise angle from the longitudinal axis of the panel. Both the radius of curvature and the panel length are 150 mm, and the panel thickness is 1 mm. The material properties used are for P3051 graphite/epoxy as

$$E_1 = 127.8 \text{ GPa}, E_2 = E_3 = 9.4 \text{ GPa}, G_{12} = G_{13} = 4.2 \text{ GPa}$$

$$G_{23} = 3.1 \text{ GPa}$$

$$\nu_{12} = \nu_{13} = 0.28, \nu_{23} = 0.52$$

$$X_T = 1726 \text{ MPa}, X_C = 1051 \text{ MPa}, Y_T = 61 \text{ MPa}$$

$$Y_C = 141 \text{ MPa}, S = 61 \text{ GPa}$$

where E_1, E_2, and E_3 are Young's moduli in the first, second, and third direction, respectively. G_{12}, G_{13}, and G_{23} are the shear moduli and ν_{12}, ν_{13}, and ν_{23} are Poisson ratios. X and Y are the strengths in the first and second direction, respectively. Subscripts T and C represent tension and compression, respectively. S is in-plane shear strength.

For $[0_3/90]_S$ cylindrical panel and $[0/\pm 45/90]_S$ plate, the following material properties are used for the comparison with the experiment and the panel thickness is 0.9 mm measured from specimen.

$$E_1 = 130.0 \text{ Gpa}, E_2 = E_3 = 10.0 \text{ Gpa}, G_{12} = G_{13} = 4.85 \text{ Gpa}$$

$$G_{23} = 3.62 \text{ Gpa}$$

$$\nu_{12} = \nu_{13} = 0.31, \nu_{23} = 0.52$$

$$X_T = 1933 \text{ MPa}, X_C = 1051 \text{ MPa}, Y_T = 51 \text{ MPa}$$

$$Y_C = 141 \text{ MPa}, S = 61 \text{ Gpa}$$

Table 1 Effect of element size on the buckling load of $[0_2/90_2]_S$ cylindrical panel using the symmetric boundary conditions for a quarter

Mesh	3 × 3	4 × 4	5 × 5	6 × 6	7 × 7	8 × 8	9 × 9
No. of active DOFs	123	224	355	516	707	928	1179
P_{cr}/A, MPa	147.3	133.8	127.1	124.4	123.5	123.2	123.1
P_{col}/A MPa	204.6	182.5	171.5	159.0	145.2	142.0	141.4

P_{cr}: Buckling load. P_{col}: Collapse load. A: Area of cross section.

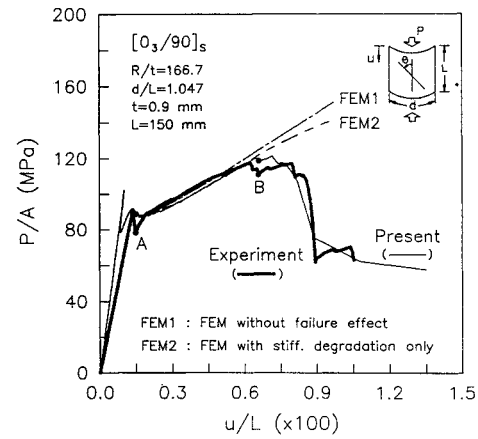

Fig. 5 Load-shortening curve of $[0_3/90]_S$ composite laminated cylindrical panel under axial compression.

The number of elements used for the finite element analysis are 16 × 16, 16 × 8, and 16 × 4 for the cylindrical panels with width-to-length ratios of 1.047, 0.524, and 0.262, respectively, which were determined by the results of mesh convergence test as shown in Table 1.

Validation of Numerical Results

Figure 5 shows the finite element and experimental load-shortening curves of the $[0/90_3]_S$ cylindrical panel. FEM1 represents the model without consideration of the effect of failure. Therefore, the stiffness degradation due to failure is not found, and the postbuckling load-carrying capacity is overestimated compared with the experiment. In FEM2, it is assumed that the stiffness of the failed layer becomes zero, but the stress carried when failure occurs is retained after the failure. Therefore, the gradient of the load-shortening curve is a little degraded with propagation of failure; nevertheless, the postbuckling load-carrying capacity is overestimated compared with experiment.

In the present model, the stress and stiffness corresponding to the failure mode are set to be zero. As shown in Fig. 5, the result of the present model is well correlated with the experiment with differences of 11% in buckling stresses and 3.1% in postbuckling compressive strength. It is presumed that the difference in the buckling stresses is due to the imperfections in geometry, material, boundary condition, and alignment. Because effects of the initial imperfections are decreased as the deflection becomes large, the difference in the load-shortening curves is reduced. Figure 6 shows the deflection contours by the finite element method and the moire fringes at the points A and B. Owing to the large difference between the bending stiffness component in axial direction D_{11} and circumferential bending stiffness D_{22} a deflection wave is formed in the axial direction at point A. As the deformation progressed, the contours developed to the straight edges with circular shapes. Figure 7 shows the load-shortening curves of the $[0/\pm 45/90]_S$ laminated plate. There is some discrepancy after the point of postbuckling compressive strength between the finite element result and experimental result because the failure model used in this paper can not consider the delamination-induced local buckling. However, in the experiment, the instantaneous collapse by the delamination-induced local buckling occurred. Therefore, the finite element result shows some discrepancy from the experimental result. Figure 8 shows the postbuckled deformed shapes at the point A in Fig. 7.

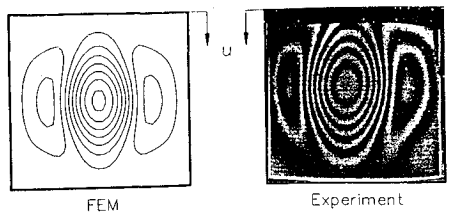

a) Point A

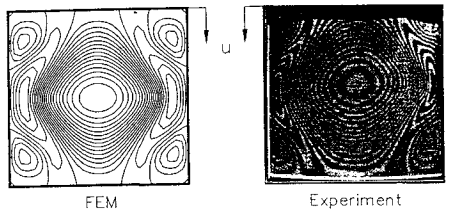

b) Point B

Fig. 6 Contour plots of deflection, w by the finite element analysis, and moire fringe patterns for $[0_3/90]_S$ cylindrical panel.

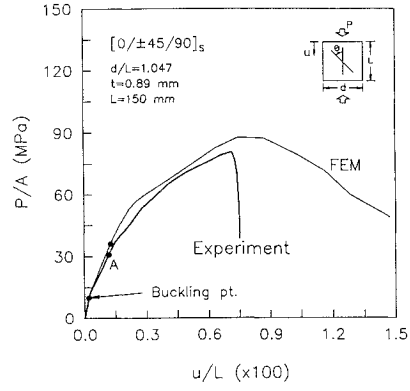

Fig. 7 Load-shortening curves of $[0/\pm 45/90]_S$ laminated plate under axial compression.

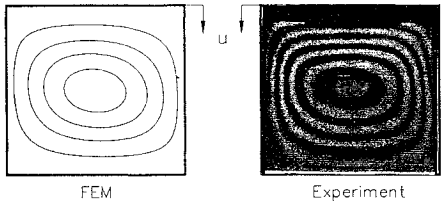

Fig. 8 Contour plots of deflection, w at point A by the finite element analysis, and moire fringe patterns for postbuckled $[0/\pm 45/90]_S$ laminated plate.

Postbuckling Compressive Strength

Figure 9 shows the buckling stress P_{cr}/A, postbuckling compressive strength P_{col}/A, and the ratio of postbuckling compressive strength to buckling P_{col}/P_{cr} for the $[0/90/\pm\theta]_S$ laminated cylindrical panels with $d/L = 1.047$. The parametric study was conducted for θ of 0, 15, 30, ..., 90 deg with a 15-deg interval. The initial buckling stress has the maximum value at $\theta = 45$ deg and the minimum value at $\theta = 0$ deg among the considered fiber angles. This shows that the buckling stress is the maximum at $\theta = 45$ deg and becomes smaller as the fiber angle θ distances from $\theta = 45$ deg. However, the postbuckling compressive strength is independent of the initial buckling stress. It has the maximum value at $\theta = 0$ deg, and becomes smaller as the fiber angle θ distances from 0 deg. This result means that the postbuckling compressive strength of the composite laminated cylindrical panel is largely dependant on the bending stiffness component in the axial direction D_{11}. Also, the ratio of postbuckling compressive strength to buckling stress is greater than 1 at $\theta = 0$ and 15 deg. This means that the cylindrical panel with the large value of bending stiffness in the axial direction

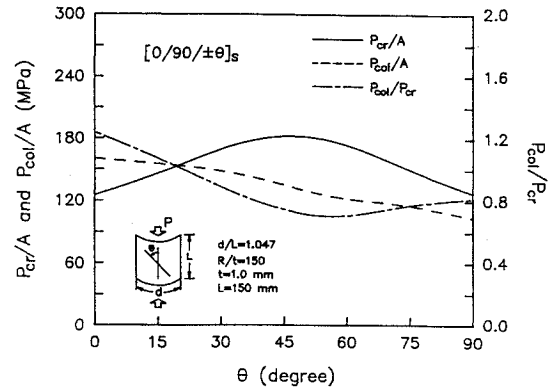

Fig. 9 Buckling stresses, postbuckling compressive strength, and the ratios of postbuckling compressive strength to buckling stress for $[0/90/\pm\theta]_S$ laminated cylindrical panels, $d/L = 1.047$.

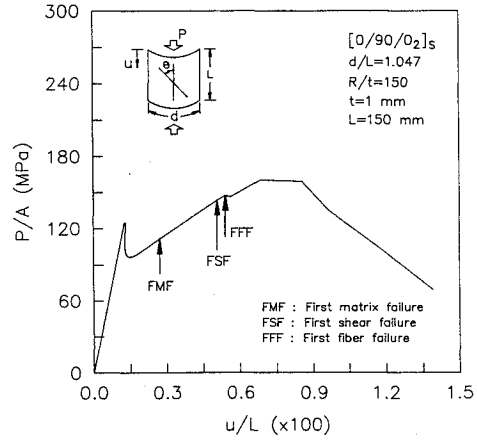

Fig. 10 Load-shortening curve for $[0/90/0_2]_S$ composite laminated cylindrical panel, $d/L = 1.047$.

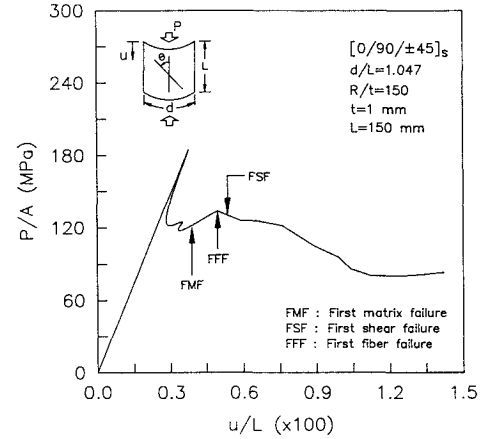

Fig. 11 Load-shortening curve for $[0/90/\pm 45]_S$ composite laminated cylindrical panel, $d/L = 1.047$.

can carry a load greater than the initial buckling load. Therefore, the safety factor for designing the composite laminated cylindrical panel should be determined with the consideration of the postbuckling strength-to-buckling stress ratio P_{col}/P_{cr}.

Figures 10 and 11 show the load-shortening curves for the laminated cylindrical panels with fiber angles $\theta = 0$ and 45 deg. As expected, the cylindrical panel with $\theta = 0$ deg supports a load greater than the initial buckling load, and the cylindrical panel with $\theta = 45$ deg experiences the first failure just after the buckling and collapses at the load extremely lower than the initial buckling load.

Figure 12 shows the buckling stress P_{cr}/A, postbuckling compressive strength P_{col}/A, and the ratio of postbuckling compressive strength to buckling P_{col}/P_{cr} for the $[0/90/\pm\theta]_S$ laminated

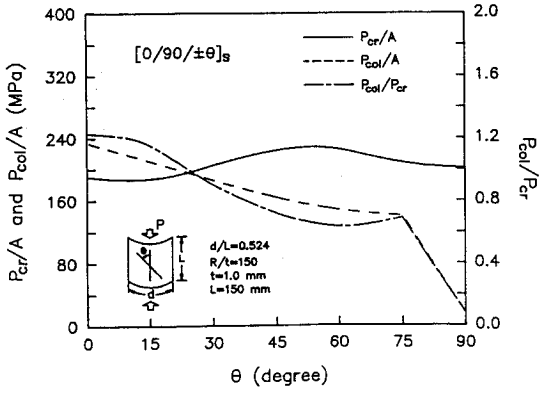

Fig. 12 Buckling stresses, postbuckling compressive strength, and the ratios of postbuckling compressive strength to buckling stress for $[0/90/\pm\theta]_S$ laminated cylindrical panels, d/L = 0.524.

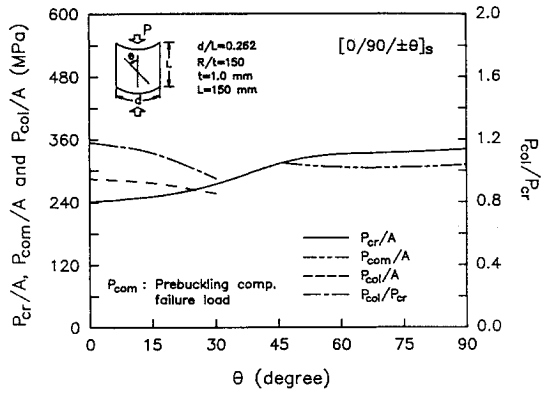

Fig. 14 Buckling stresses, postbuckling compressive strength, and the ratios of postbuckling compressive strength to buckling stress for $[0/90/\pm\theta]_S$ laminated cylindrical panels, d/L = 0.262.

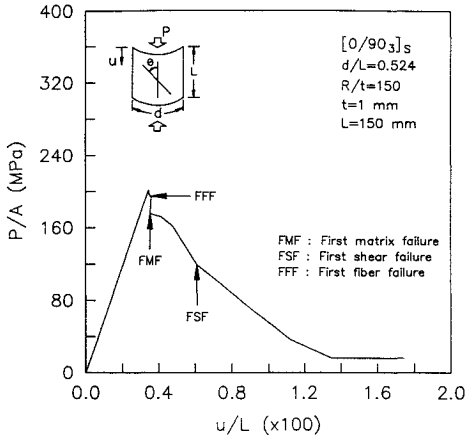

Fig. 13 Load-shortening curve for $[0/90_3]_S$ composite laminated cylindrical panel, d/L = 0.524.

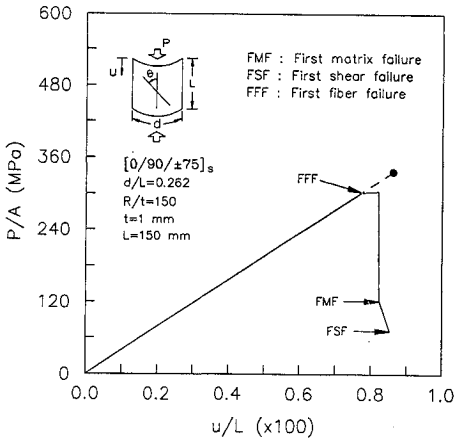

Fig. 15 Load-shortening curve for $[0/90/\pm 75]_S$ composite laminated cylindrical panel, d/L = 0.262.

cylindrical panels with width-to-length ratio, $d/L = 0.524$. The trend of buckling stress is similar to the cylindrical panels with $d/L = 1.047$. However, the effect of fiber angle θ on the buckling stress is smaller than in the cylindrical panel with $d/L = 1.047$. Furthermore, the maximum buckling stress is obtained at $\theta = 60$ deg. This means that the effect of circumferential bending stiffness D_{22} on buckling stress is enlarged in the cylindrical panels with small width-to-length ratio. Because of the effect of constraints along the straight edges the magnitude of the buckling stress is greater than in the cylindrical panel with $d/L = 1.047$. However, even in the cylindrical panels with $d/L = 0.524$, the postbuckling compressive strength is independent of the buckling stress, and dominated by only one parameter, namely, bending stiffness in the axial direction D_{11}. Also, the ratio of postbuckling strength-to-buckling stress shows a trend similar to the cylindrical panels with $d/L = 1.047$. An especially interesting result is obtained at $\theta = 90$ deg. As shown in Fig. 13, in the $[0/90_3]_S$ cylindrical panel, the first fiber failure occurs just after passing the buckling point, and it results in the collapse. In this case the buckling means the collapse.

Figure 14 shows the results for slender $[0/90/\pm\theta]_S$ cylindrical panels with $d/L = 0.262$. As shown in the figure, the maximum buckling stress is obtained at $\theta = 90$ deg, and followed by 60, 75, 45, 30, 15, and 0 deg in order of their magnitude. This result shows that as the width-to-length ratio becomes smaller, the effect of circumferential bending stiffness D_{22} on buckling stress is enlarged. In the $[0/90/\pm\theta]_S$ cylindrical panels with θ greater than 45 deg, it should be noted that prebuckling static compressive failure occurs before the buckling and directly results in catastrophic structural failure. The prebuckling compressive failures occur just before the buckling when $\theta = 45$ deg and at the stress of 85% of buckling stress when $\theta = 60$, 75, and 90 deg. This phenomena contradicts common sense in that the shell structure subjected to the axial compression usually has buckling stress lower than the static compressive strength. Therefore, in designing the cylindrical panels with high buckling stress, the static compressive strength should be considered. Figure 15 shows the typical load-shortening curve of $[0/90/\pm 75]_S$ cylindrical panel which has prebuckling compressive failure. The postbuckling compressive strength of the cylindrical panels in which the prebuckling compressive failure is not found is determined by the axial bending stiffness D_{11}.

Conclusions

A modified arc-length method combined with the most conservative progressive failure model was introduced into the nonlinear finite element method. The finite element analysis was performed to characterize the postbuckling compressive strength of laminated composite cylindrical panels. The numerical results were compared with experimental results for a $[0_3/90]_S$ cylindrical panel and a $[0/\pm 45/90]_S$ plate and show excellent agreement with $[0_3/90]_S$ cylindrical panel. In the $[0/\pm 45/90]_S$ plate, some difference was obtained after collapse due to the delamination of the specimen.

The buckling loads of $[0/90/\pm\theta]_S$ cylindrical panels were greatly affected by the fiber angle θ and width-to-length ratio, but the postbuckling compressive strength is dominated only by the bending stiffness in axial direction. In several cylindrical panels with small width-to-length ratio, prebuckling compressive failure was detected.

References

[1]Hutchinson, J. W., and Koiter, W. T., "Postbuckling Theory," *Applied Mechanics Reviews*, Vol. 23, 1976, pp. 1353–1366.

[2]Steplens, W. B., "Imperfection Sensitivity of Axially Compressed Stringer Reinforced Cylindrical Panels under Internal Pressure," *AIAA Journal*, Vol. 9, No. 9, 1971, pp. 1713–1719.

[3]Jun, S. M., and Hong, C. S., "Buckling Behavior of Laminated Composite Cylindrical Panels under Axial Compression," *Computers and Structures*, Vol. 29, No. 3, 1988, pp. 479–490.

[4]Hong, C. S., and Jun, S. M., "Buckling Behavior of Laminated Composite Cylindrical Panel with Initial Imperfections," *Recent Developments in Buckling of Structures*, PVP-Vol. 183, AD-Vol. 18, American Society of Mechanical Engineers, 1989, pp. 9–15.

[5]Sheinman, I., Shaw, D., and Simitses, D. J., "Nonlinear Analysis of Axially-Loaded Laminated Cylindrical Shells," *Computers and Structures*, Vol. 16, No. 1–4, 1983, pp. 131–137.

[6]Wilkins, D. J., "Compression Buckling Tests of Laminated Graphite-Epoxy Curved Panels," *AIAA Journal*, Vol. 13, No. 4, 1975, pp. 465–470.

[7]Bauld, N. R., Jr., and Khot, N. S., "Numerical and Experimental Investigations of the Buckling Behavior of Composite Panels," *Computers and Structures*, Vol. 15, No. 4, 1982, pp. 393–403.

[8]Khot, N. S., and Bauld, N. R., Jr., "Further Comparison of the Numerical and Experimental Buckling Behaviors of Composite Panels," *Computers and Structures*, Vol. 17, No. 1, 1983, pp. 61–68.

[9]Snell, M. B., and Morley, N. T., "The Compression Buckling Behavior of Highly Curved Panels of Carbon Fibre Reinforced Plastic," *Proceedings of the 5th International Conference on Composite Materials*, Vol. 5 (San Diego, CA), 1985, pp. 1327–1354.

[10]Knight, N. F., Jr., Starnes, J. H., Jr., and Waters, W. A., Jr., "Postbuckling Behavior of Selected Graphite-Epoxy Cylindrical Panels Loaded in Axial Compression," AIAA Paper 86-0881, May 1986.

[11]Engelstad, S. P., Reddy, J. N., and Knight, N. F., Jr., "Postbuckling Response and Failure Prediction of Graphite-Epoxy Plates Loaded in Compression," *AIAA Journal*, Vol. 30, No. 8, 1992, pp. 2106–2113.

[12]Kweon, J. H., and Hong, C. S., "Postbuckling Analysis of Composite Laminated Cylindrical Panels under Axial Compression," *AIAA Journal*, Vol. 31, No. 8, 1993, pp. 1535–1537.

[13]Bathe, K. J., *Finite Element Procedures in Engineering Analysis*, Prentice-Hall, Englewood Cliffs, NJ, 1982.

[14]Jones, R. M., *Mechanics of Composite Materials*, McGraw-Hill, New York, 1975.

[15]Chou, S. C., Orringer, O., and Rainey, J. H., "Post-Failure Behavior of Laminates. I—No Stress Concentration," *Journal of Composite Materials*, Vol. 10, 1976, pp. 371–381.

[16]Hahn, H. T., and Tsai, S. W., "On the Behavior of Composite Laminates after Initial Failures," *Journal of Composite Materials*, Vol. 8, 1974, pp. 288–305.

[17]Tsai, S. W., *Composite Design*, 4th ed., Dayton, OH, 1988.

[18]Crisfield, M. A., "A Fast Incremental/Iterative Solution Procedure That Handles Snap-Through," *Computers and Structures*, Vol. 13, 1981, pp. 55–62.